A Spectroscopic Analysis of the Stress Distribution along the Reinforcement Fibers in Model Composites: End Effects

Cun F. Fan and Shaw L. Hsu*

Polymer Science and Engineering Department and The Materials Research Laboratory, The University of Massachusetts, Amherst, Massachusetts 01003. *Received June 9, 1988; Revised Manuscript Received September 8, 1988*

ABSTRACT: A Raman-mechanical technique has been applied to analyze the stress distribution along the reinforcement fiber in a model composite. This technique has demonstrated high sensitivity and spatial resolution and was used to show significantly different stress distribution exists along reinforcement fibers of different ends, tapered or blunt, when the composites experience tensile or compressive stress. For the fibers with blunt ends, the stress distribution measured agrees well with previous experimental studies and calculated results. However, for fiber with tapered ends, a totally different stress distribution curve was found. In this case the stress distribution measured is a constant along the fiber and a critical length was not found. Higher stress transfer efficiency was explained on purely geometric considerations.

Introduction

The basic reinforcement mechanism associated with composites incorporating discontinuous fibers is the transfer of applied stress from the matrix to the fiber through the shear stress at the interface.[1] The stress transfer mechanism and the resultant stress distribution have been extensively studied both theoretically and experimentally. Since the model first proposed by Cox in 1952,[2] several others have been developed making analytical solutions available to model the transfer mechanism.[3-8] The development of advanced computation capabilities also make it possible to use the engineering stress analysis methods, mainly finite element method[9] and finite difference approach[10] to calculate the stress distribution in fibers and matrix. Most of the experimental studies, however, are limited to the stress analysis of the matrix.[11-14] Until recently, there have been few direct experimental techniques with sufficient sensitivity and spatial resolution to demonstrate the stress distribution expected for individual fibers in composites.[15-17]

The available experimental data agree well with the predicted distribution. The stress distribution along the fiber shows the tensile stress to be zero or very small at the fiber ends and then increases rapidly toward the middle of the fiber reaching a plateau when the distance from the ends is larger than $l_c/2$, where l_c is defined to be the critical length of the system. The interface shear stress has a maximum value at fiber ends and then decreases rapidly toward the middle of the fiber reaching zero when the distance exceeds $l_c/2$. This description is applicable for fibers of uniform diameter and square ends.

Several aspects of the distribution described above need to be considered further. First, the fiber must be longer than the critical length; otherwise the fiber cannot carry the maximum load. Even if the fiber length is longer than l_c, the average load on fiber is always lower than expected for a continuous fiber due to end effects. Second, high interface shear stress may cause interface failure and the section of the fiber near the ends are most likely to fail. Once it occurs, the interface failure may grow along the fiber reducing the ability to transfer stress. Third, under load, high stress concentration, approximately three times the average, near fiber ends may cause matrix yield (for ductile matrix) or fracture (for brittle matrix).[11] It is rather clear that both the fiber/matrix interface and the matrix near fiber ends are most vulnerable to structural failure and need to be characterized carefully.

As mentioned above, most of the studies deal with fibers of uniform diameter; therefore, it would be interesting to investigate the effects of different fiber geometric parameters. Modification of the effective stress distribution or possible elimination of the problems associated with sections of high stress and inefficiency in stress transfer may be possible. Whether changing fiber shape can indeed improve reinforcement property is still not well-defined. Previous photoelastic study and finite element analysis have suggested that the stress concentration near the fiber end can be reduced if the fiber has a sharp tapered end geometry.[9,12] Other studies, however, are inconsistent with such a conclusion.[18] All those studies considering the effects of fiber geometry were directed at the stress distribution at the fiber/matrix interface or matrix. In fact, no experimental data are available to elucidate the stress distribution on the fiber. We feel this is a very important aspect of the problem and more experimental studies are necessary. In this study, we report the use of a Raman-mechanical technique to examine the stress distribution along the fiber. The distribution results from thermal residual stress, compressive in nature, and an applied tensile stress for fibers of blunt ends and tapered ends. We found some very unusual although easily understood stress distribution curves. Our results are reported here.

Experimental Section

Calibration and Measurement of Stress Distribution. Although photoelastic technique has been used to measure the stress distribution on fiber,[19] a direct description of stress distribution along the reinforcement fiber under the mechanical strain has only become available by using a combination of Raman-mechanical technique.[15-17] In this case, we were able to achieve extremely high spatial resolution without the need to use microprobe technique. When selected carefully, no fluorescence was observed in the fiber sample, the amorphous matrix and the accelerator used for curing.

The validity of the technique is based on knowing the linear relationship between the C≡C backbone stretching frequency of a fiber-like polydiacetylene single crystal and the effective sample strain.[20] The stress distribution was then obtained by measuring the C≡C vibration frequency from point to point along fiber when the composite is stressed by mechanical means. Residual stress due to curing shrinkage and differences in expansion coefficients between the matrix and the fiber, existing even for sample cured at room temperature, also needs to be considered. The evaluation of the stress distribution involves a direct comparison of the C≡C frequency for the fiber, fiber embedded in the cured clear amorphous matrix, and the stressed composite sample by point-by-point subtraction. For our experiment to be quantitatively meaningful, particularly considering the effects arising from the two types of stresses needs to be separated, exact,

* To whom correspondence should be addressed.

0024-9297/89/2222-1474$01.50/0

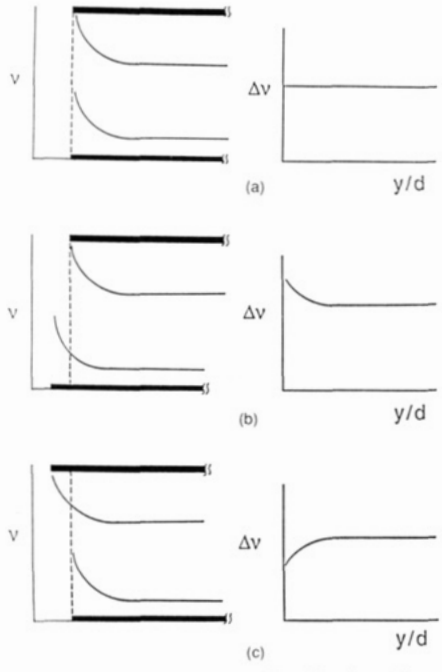

Figure 1. Measurement of stress distribution along the fiber: (a) shows when the end of the fiber was accurately determined a true distribution curve can be obtained; (b) and (c) show two cases of incorrect measurement (missing the fiber end in one of the two measurements), incorrect stress distribution curves are then obtained. In all three cases, the $\Delta\nu$ represents the difference between the measured values before and after strain was applied.

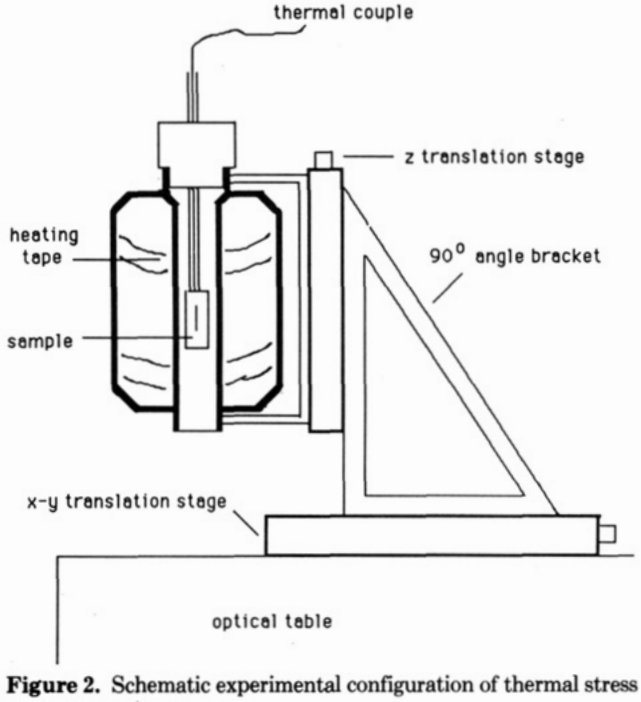

Figure 2. Schematic experimental configuration of thermal stress measurements.

and reproducible determination of the position along the fiber is necessary. The most convenient method for such measurement is to measure the position relative to the ends of the fiber. The possible errors, however, are shown schematically in Figure 1. If the positions are not determined accurately, the stress distribution obtained may lead to completely erroneous conclusions.

Therefore, considerable attention was given to the construction of a "sample holder", for both the temperature variation and stretching experiments, to enable us to move the composite sample in the Raman sample chamber with great precision as shown in Figure 2 and 3. The position along fiber can be determined reproducibly within 10 μm.

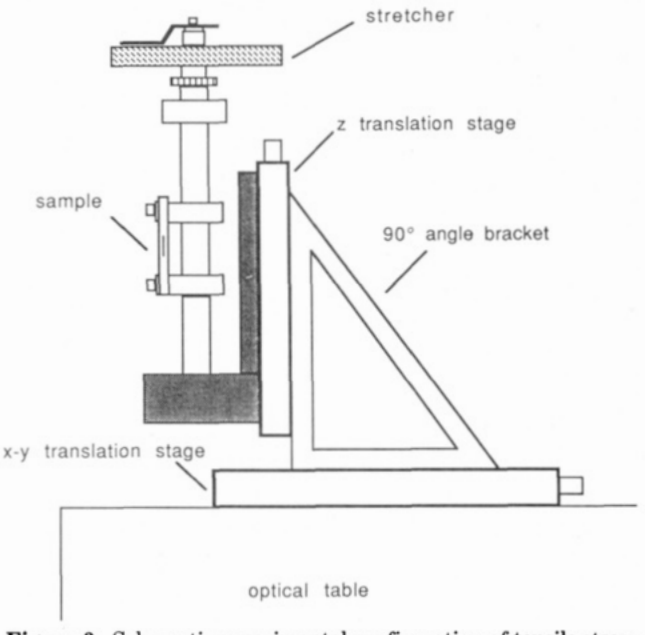

Figure 3. Schematic experimental configuration of tensile stress measurements.

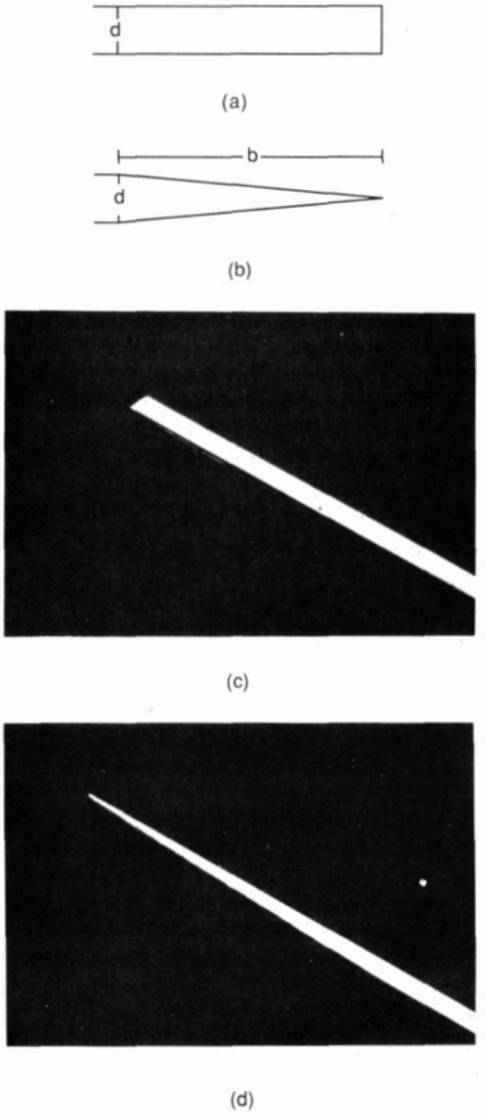

Figure 4. Schematic drawings and photographs of the two types of fibers used in this study: (a) blunt ended fiber; (b) taper ended fiber; (c) photograph of an actual blunt ended fiber; (d) photograph of a tapered ended fiber.

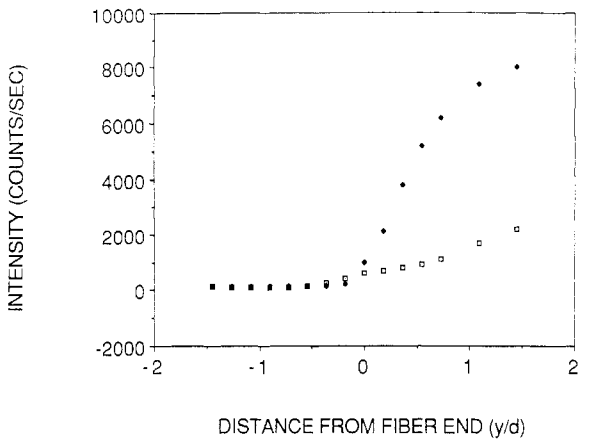

Figure 5. Raman scattering intensity of C≡C stretching as a function of distance from fiber ends: (◆) blunt ended fiber; (⊡) taper ended fiber.

Schematic drawings and photographs of the blunt and tapered fibers used in our experiment are shown in Figure 4. The reference point for each stress distribution measurement, the fiber end, can be determined simply by measuring the scattering intensity of the C≡C vibration as we move the fiber at the focus of the incident laser beam. The end for the blunt end fiber can be determined easily by monitoring the scattering intensity. The gradual increasing scattering intensity for the tapered end can be observed clearly as well. Typical data are shown in Figure 5. In either case, the fiber ends can be determined with a great deal of confidence.

Sample Preparation. The polydiacetylene fiber used in our experiments is p-HDU which was prepared in our laboratory as described previously.[21] Epon 828 was used as matrix and DETA as curing agent. The sample for studying thermal induced stress was cured at 55 °C for 24 h. After curing, stress distribution were also measured at 38 and then 18 °C. Most model composites used in the stretching experiment were cured at room temperature for approximately 25 days. Some were prepared at 55 °C for comparison.

Most of the p-HDU single crystal fibers have tapered ends, but some blunt ended fibers can be found as well. The diameter of individual fibers, d, is approximately 0.07 mm. The actual cross section area of fiber is not circular but more rectangular in shape. Only fibers which have both well defined ends and are defect-free were used. For the tapered end fiber the ratio of b/d is approximately 15.

The Raman spectrometer used in the experiments was a Jobin Yvon Model HG.2S instrument. A He-Ne laser tuned to the 6328-Å line was used as the Raman excitation source. Neutral density filters were used to reduce the laser power to less than 5 mW at the sample to prevent damage from laser heating.

Results and Discussions

Thermal Induced Stress Distribution. It has been well established that due to the mismatch of thermal expansion coefficients between the p-HDU and epoxy matrix, evidence of compressive residual stress will be present when the composite cools from higher curing temperature to lower temperatures.[21] The shear stress at the fiber matrix interface leads to the existence of longitudinal stress distribution along the fiber.[19] The samples were cured at 55 °C and then cooled to 37 and 19 °C. The measured C≡C frequencies for three temperatures, as a function of distance from the end of a blunt ended or tapered ended fiber, are shown in Figure 6. Each set of data was plotted in terms of a dimensionless parameter y/d, where y is the absolute distance from fiber end and d is the diameter of fiber. Because the diameter of tapered ended fiber is constantly changing near fiber end, d, in this case, is the diameter of fiber in the middle part which is a constant when y is larger than b. We have elected to use this

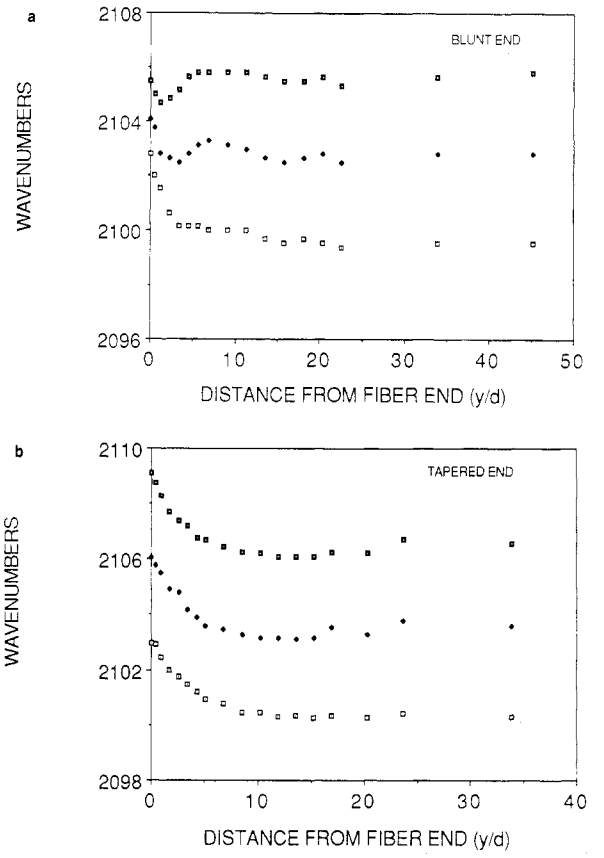

Figure 6. C≡C stretching vibration frequency measured along fiber for three different temperatures: (a) blunt ended fiber; (b) tapered ended fiber; (⊡) 55 °C; (◆) 37 °C; (□) 19 °C.

normalized displacement (y/d) since there are variations in the fiber dimension even under the most controlled circumstances.

It is clear both types of fibers in the cured matrix are not stress free. It is equally clear that the frequency/stress distributions for the two types of fibers have totally different responses to the virtually identical thermal history. The frequency measured near the middle of the fiber at the curing temperature 55 °C is quite close to the unperturbed value measured for a fiber outside the matrix. The C≡C frequency measured near the fiber ends at that temperature, however, depart from the isolated fiber significantly showing most of the residual stress build-up during curing process are concentrated near the ends. The data are most conveniently presented by taking the difference of the two lower temperature measurements relative to the curing temperature as shown in Figure 7. Here $\Delta\nu$ is defined as $\nu - \nu_c$ where ν_c is the frequency at curing temperature. These curves represent the thermal stress distribution due to a temperature drop. For the tapered ended fiber, the C≡C frequency difference remains essentially unchanged along the fiber showing the stress is distributed evenly. In contrast, the frequency difference of the fiber with blunt ends changes along the fiber indicating an uneven stress distribution. The maximum effective compressive strain is approximately 0.15% for ΔT = 18 °C and 0.3% for ΔT = 36 °C respectively.

The different thermal induced stress distribution found between the blunt and tapered ended fibers is significant. For the blunt ended fiber, the stress increases gradually from the fiber end reaching the maximum value at $^1/_2 l_c$. If we consider the analogy between tensile transfer and compressive stress transfer, this kind of distribution is expected from theoretical calculations and agree well with other experimental observations. In this case, fiber ends

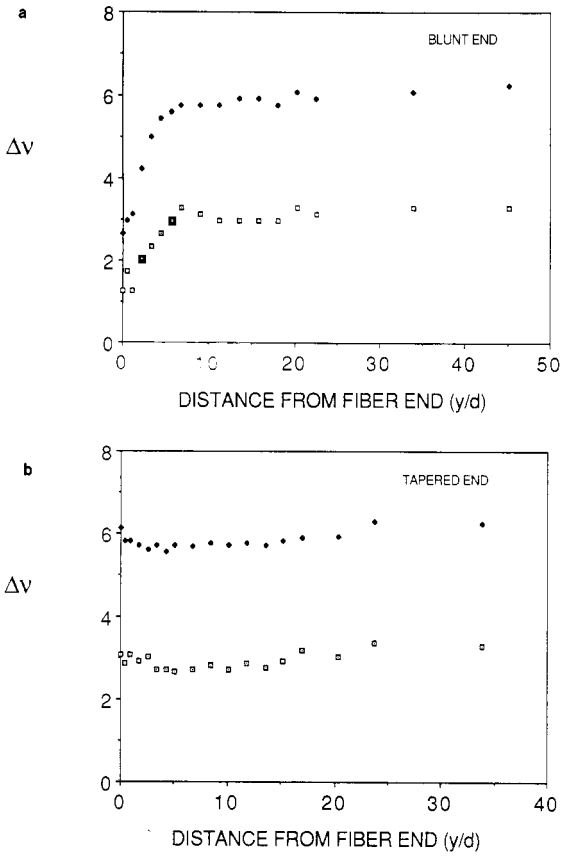

Figure 7. C≡C stretching vibration frequency difference due to temperature drop as a function of distance from fiber ends: (a) blunt ended fiber; (b) tapered ended fiber; (⊡) ΔT = 18 °C; (◆) ΔT = 36 °C.

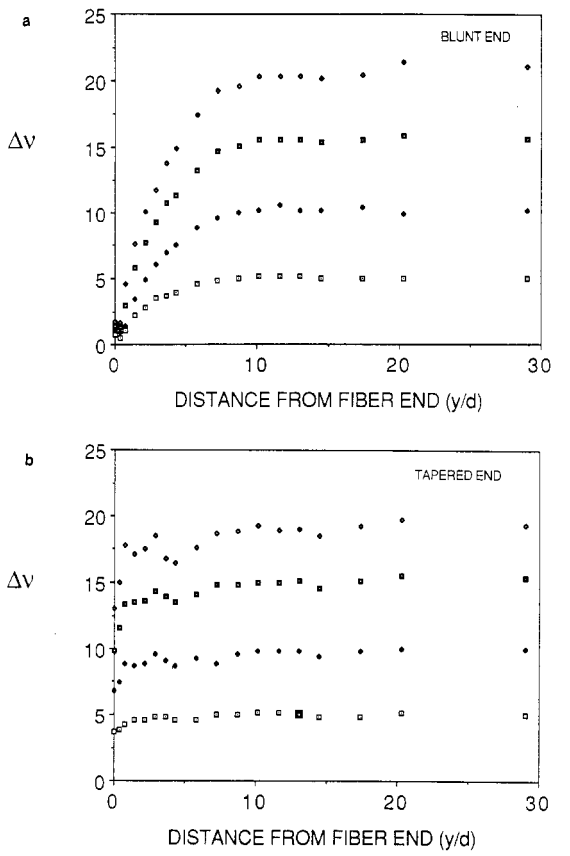

Figure 8. C≡C stretching vibration frequency difference measured along the fiber for four strain values: (a) blunt ended fiber; (b) tapered ended fiber; (⊡) 0.25%; (◆) 0.50%; (□) 0.75%; (◇) 1.00%.

carry less load. Unlike blunt ended fiber, for the tapered ended fibers, there is no critical length in the stress distribution. Even at the extreme ends, each section of the fiber is capable of carrying load along the fiber axis. Although the relative advantages of having different fiber ends have been discussed in few studies,[9,12] no such stress distribution curves on fibers have actually been reported.

Tensile Stress Distribution. The interesting differences found for the thermal induced stress distribution lead us to examine in greater detail the effect of fiber end geometry on the tensile stress distribution. The C≡C stretching frequency differences as a function of distance from fiber end for four different strain values are plotted in Figure 8. The difference found for the two types of fibers is obvious. It should be emphasized that both samples were cured at room temperature. The effect of curing stress, which is much smaller than higher temperature cured sample, has been eliminated by plotting $\Delta\nu$ as a function of distance from fiber ends. In these plots, $\Delta\nu$ is defined as $\nu_{\epsilon 0} - \nu_{\epsilon}$, where $\nu_{\epsilon 0}$ is the C≡C frequency measured at zero composite strain. Again, fibers of different ends have completely different stress distribution curves.

Since the first stress distribution theory was proposed in 1952,[2] it has been generally accepted that for discontinuous fibers, the length of fiber must exceed the critical length l_c in order to act effectively as reinforcement. Next to the most simplistic assumption that stress increases linearly with distance from fiber ends, the hyperbolic cosine shape curve is the basic description of the tensile stress distribution on the fiber. From our experimental data, we derive a totally different picture of stress distribution for the tapered ends. In this case, no critical length is necessary. The average stress on the tapered ended fiber is almost equal to the continuous fiber, higher than that of the blunt end fiber.

The observed tensile stress distribution curve for the blunt ended fiber has been predicted and agrees well with other experimental results. The tensile stress increases gradually from fiber ends reaching a plateau when the distance from fiber end exceeds half of the critical length l_c. This tensile stress distribution curve can be characterized by three parameters: the plateau value, critical length, and the stress value at fiber ends.

As predicted, the maximum strain value ϵ_{max} observed in our experiments is nearly equal to the overall strain of composite and the maximum stress is $E_f\epsilon_{max}$, where E_f is the fiber modulus. The critical length l_c or relative critical length l_c/d_f (d_f is the diameter of fiber) observed usually do not agree well with theoretical predictions. For example, l_c in the Cox's theory[2] is given by

$$\frac{1}{\cosh(\beta(l_c/2))} = 1 - \frac{E_m}{E_f} \tag{1}$$

where $\beta = (H/AE)^{1/2}$, $H = 2\pi G_m/\ln(r_0/r_f)$, $E = E_f - E_m$, and $A = \pi r_f^2$. E_f and E_m are the modulus of fiber and matrix respectively, r_f is the radius of fiber, r_0 is the mean separation between fibers which equal half width of matrix for single fiber system, and G_m is the shear modulus of matrix which is approximately taken to be $E_m/3$. We obtain the relative critical length

$$\frac{l_c}{d_f} = \left(\frac{3}{2}\ln\frac{r_0}{r_f}\right)^{1/2}\left(\frac{E_f - E_m}{E_m}\right)^{1/2}\cosh^{-1}\left(\frac{E_f}{E_f - E_m}\right) \tag{2}$$

In our model composite, r_0/r_f = 43, E_f/E_m = 10, and the calculated value of l_c/d_f from eq 2 should be approximately 3.33 quite different from our experimental data, ~20. If the shape of the cross sectional area of fiber, i.e. the cross

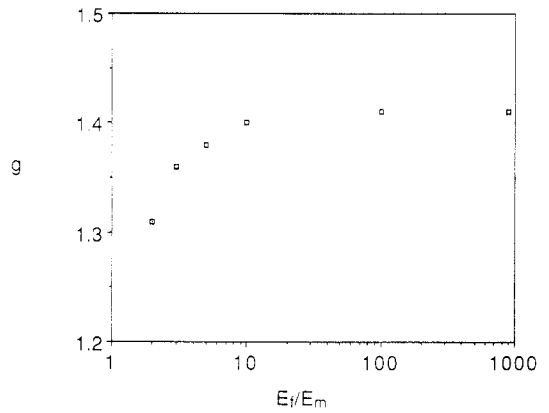

Figure 9. g parameter as a function of E_f/E_m.

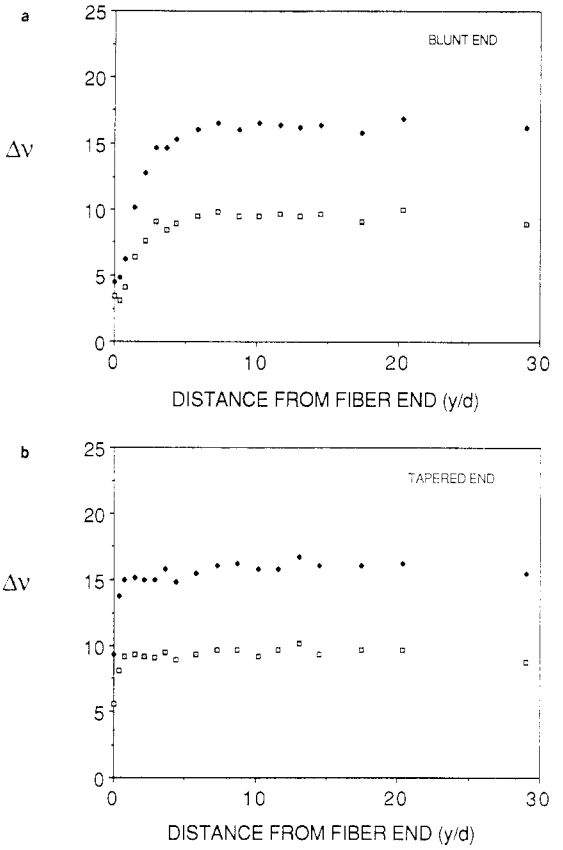

Figure 10. C≡C stretching vibration frequency difference measured along the fiber for two strain values: (a) blunt ended fiber; (b) tapered ended fiber. Both samples were cured at 58 °C; (⊡) 0.50%; (◆) 0.80%.

section area of p-HDU fiber, is not round but rectangular, the difference becomes even larger.

Equation 2 shows that l_c/d_f is a function of r_0/r_f and E_f/E_m. Actually, it is only a function of r_0/r_f because the term related to E_f/E_m, defined as

$$g = \left(\frac{E_f - E_m}{E_m}\right)^{1/2} \cosh^{-1}\left(\frac{E_f}{E_f - E_m}\right)$$

changes very little as a function of E_f/E_m as shown in Figure 9. l_c/d_f should then be a constant in our experiments. Instead, we found that l_c/d_f will change under some curing conditions even if the r_0/r_f remains unchanged. The $\Delta\nu$ distributions along fiber at two strain values for blunt and tapered ended fiber are shown in Figure 10. These samples were cured at 58 °C and stretched at room temperature. Our previous studies have shown that compressive failure will not occur at this curing temperature.[21]

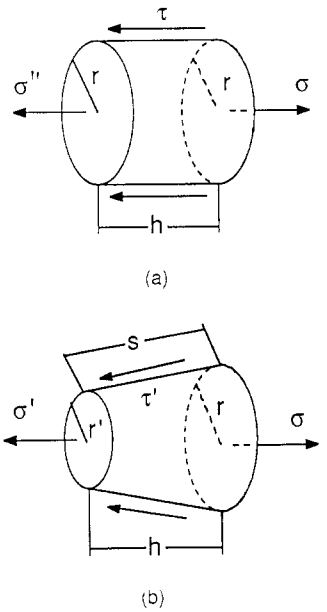

Figure 11. Stress balance of two small elements of fibers: (a) blunt ended fiber; (b) tapered ended fiber.

The effective thermal residual stress distribution can be eliminated with the method mentioned in the Experimental Section. The distribution functions are similar to that of room-temperature cured samples except for the blunt end fiber. For this sample, the l_c/d_f is ~12, smaller than the value for the sample cured at room temperature. However, the exact reasons for this difference is not clear. This difference may be explained by an increase in the radial frictional force which greatly enhances the interface adhesion. Our previous studies, however, showed interface adhesion is excellent even for the sample cured at room temperature. Furthermore, the thermal expansion coefficients of the fibers and the matrix do not suggest a higher friction for samples cured at higher temperatures.[21]

The third parameter commonly used to characterize the stress distribution curve is the stress transfer at the fiber ends. Most theories assume that stress transfer at fiber ends is zero. The calculated results have shown that the end contribution can be 20% or in some cases more then 25% of maximum stress.[9,10] Our results suggest that for samples cured at room temperature, strains at the ends are very small and remain essentially constant when the overall composite strain increases. For higher temperature cured samples, the end contribution becomes more significant and can reach a range of 20–30% of the maximum fiber strain. Higher curing temperature seems to increase the stress transfer efficiency of blunt end fibers by decreasing the critical length and increasing the stress transfer through fiber end. But it may also increase the chance having fiber compressive failure if the use temperature is well below the curing temperature.

Explanation of End Effects. To our knowledge no theoretical treatment of stress distribution in reinforcement fibers have considered the tensile stress distributions associated with tapered ended fibers. Previous finite element analysis carried out have considered the geometric effect of fiber end but have not provided the needed tensile stress distribution curve.[9] A complete explanation of the observed stress distribution in tapered end fiber really needs additional detailed analysis. It is useful and possible, however, to explain these end effects from a more qualitative perspective.

Let us consider two small elements of fiber as shown in Figure 11, one for blunt end and one for tapered end. The

right-hand side of both elements have same radius r and experience a tensile stress σ. The tensile stress on the left-hand sides are σ' and σ''. The force balance equation along the fiber axis is

$$\sigma''\pi r^2 + \tau\pi 2rh = \sigma\pi r^2 \tag{3}$$

for blunt fiber and

$$\sigma'\pi r'^2 + \tau'\pi(r + r')s\cos\theta = \sigma\pi r^2 \tag{4a}$$

or

$$\sigma'\pi r'^2 + \tau'\pi(r + r')h = \sigma\pi r^2 \tag{4b}$$

for tapered ended fiber, where $h = s\cos\theta$ is the projection of s in the fiber axis direction. By assuming $\tau = \tau'$, the relative stress value for the two types of fibers is

$$\sigma' = \sigma''\left(\frac{r}{r'}\right)^2 + \tau h\frac{r - r'}{r'^2} \tag{5}$$

if $(r/r')^2 > 1$ and $\tau h(r - r')/r'^2 > 0$, then $\sigma' > \sigma''$.

The critical assumption of the derivation is for $\tau = \tau'$. This certainly is not true in all circumstances. If $\tau < \tau'$, it would be difficult to explain our results by this simple consideration. Previous experimental results, however, suggest that $\tau > \tau'$.[12] If this is the case, $\sigma' > \sigma''$ will be consistent with our experimental data.

On the basis of our experimental observation the $\sigma' = \sigma$ for tapered ended fiber, from the eq 4b, we obtain

$$\tau' = \frac{\sigma(r - r')}{h} = \sigma\frac{dx}{dy} \tag{6}$$

This result suggests that at any position along the fiber matrix interface, for tapered ended fiber the shear stress is proportional to the slope of the interface relative to fiber axis. This implies the sharper the fiber ends, the smaller the interface shear stress. This conclusion agrees well with the one derived with more sophisticated finite element analyses. Although our explanation may be too simplistic, the basic reason for higher stress transfer efficiency of tapered ended fiber is clear. It is a purely geometric effect that a smaller cross area has a higher stress if the load is same.

Conclusions

Both thermal (compressive) stress and tensile stress distributions along the reinforcement fiber in a single fiber model composite have been examined with a Raman-mechanical technique. To our knowledge, the significant effects of fiber end geometry on the stress transfer efficiency were observed for the first time. For the fiber with a uniform radius, the stress distribution curve is similar to other observations and qualitatively agree well with theoretical predictons. A completely different stress distribution curve has been observed in the tapered ended fiber in both thermal and stretching experiments. In this case the stress is uniform along the fiber and no critical length exists. The higher stress transfer efficiency of tapered fiber was attributed to a purely geometric effect.

Acknowledgment. This study has been supported by the donors of the Petroleum Research Fund, administered by the American Chemical Society.

Registry No. (DETA)(Epon 828) (copolymer), 31326-29-1.

References and Notes

(1) Holister, G. S.; Thomas, C. *Fibre Reinforced Materials*; Elsevier: Amsterdam, 1966.
(2) Cox, H. L. *Br. J. Appl. Phys.* **1952**, *3*, 72.
(3) Outwater, J. O., Jr. *Mod. Plast.* **1956**, March, 56.
(4) Dow, N. F. *G.E.C. Missile and Space Division*, Report No. R63SD61, 1963.
(5) Rosen, B. W. In *Fiber Composite Materials*; ASM: Metals Park, OH, 1965; Chapter 3.
(6) Kelly, A.; Tyson, W. R. *J. Mech. Phys. Solids* **1965**, *13*, 392.
(7) Amirbayat, J.; Hearle, J. W. S. *Fibre Sci. Technol.* **1969**, *2*, 123.
(8) Piggott, M. R. *Load Bearing Fibre Composites*; Pergamon Press: Oxford, 1980.
(9) Carrara, A. S.; McGarry, F. J. *J. Compos. Mater.* **1968**, *2*, 222.
(10) Termonia, Y. *J. Mater. Sci.* **1987**, *22*, 504.
(11) Tyson, W. R.; Davies, G. J. *Br. J. Appl. Phys.* **1965**, *16*, 199.
(12) Schuster, D. M.; Scala, E. *Transition Met. Soc. AIME* **1964**, *230*, 1635.
(13) Mclaughlin, T. F. *J. Compos. Mater.* **1968**, *2*, 44.
(14) Mclaughlin, T. F.; Barker, R. M. *Exp. Mech.* **1972**, *4*, 178.
(15) Galiotis, C.; Young, R. J.; Yeung, P. H.; Batchelder, D. N. *J. Mater. Sci.* **1984**, *19*, 3640.
(16) Kim, P. K.; Xu, Y. Y.; Chang, Chih; Hsu, S. L. *Polymer* **1986**, *27*, 1547.
(17) Robinson, I. M.; Young, R. J.; Galiotis, C.; Batchelder, D. N. *J. Mater. Sci.* **1987**, *22*, 3642.
(18) Mclaughlin, T. F. *Exp. Mech.* **1966**, *10*, 481.
(19) Haslett, W. H.; McGarry, F. J. *Mod. Plast.* **1962**, December, 135.
(20) Mitra, V. K.; Risen, W. M., Jr.; Baughman, R. H. *J. Chem. Phys.* **1977**, *66*, 2731.
(21) Fan, C. F.; Hsu, S. L. *J. Polym. Sci. Phys.*, in press.